Spectrochimica Acta Part B: Atomic Spectroscopy 209 (2023) 106786

Contents lists available at ScienceDirect

Spectrochimica Acta Part B: Atomic Spectroscopy

journal homepage: www.elsevier.com/locate/sab

Solution-cathode glow discharge under high NaCl concentration: Impact on excitation conditions and analyte transfer processes

Jaime Orejas *, Yinchenxi Zhang, Cristian Soto-Gancedo, Luis Javier Fernández-Menéndez, Jorge Pisonero *, Nerea Bordel

Grupo de Espectroscopia, Láseres y Plasmas (GELP), Department of Physics, University of Oviedo, C/ Gonzalo Gutiérrez Quirós S/N, Mieres 33600, Spain

ARTICLE INFO

Keywords:
Plasma-liquid interaction
Solution cathode glow discharge
Optical emission spectrometry
Elemental analysis
Atmospheric pressure glow discharge

ABSTRACT

The Solution-Cathode Glow Discharge (SCGD) is a useful plasma source for elemental analysis, gathering atomization/excitation/ionization capabilities for aqueous solutions with simplicity and low consumption. When combined with Optical Emission Spectrometry (OES), ng/mL limits of detection can be achieved for multiple elements. Additionally, this plasma source presents certain robustness against the presence of dissolved non-analyte ions. Nevertheless, the mechanisms by which the SCGD can transfer the dissolved analytes from the solution into the plasma, and the mechanisms of how concomitant ions in the sample solution affect the performance of the analysis, are still not fully understood. Therefore, fundamental plasma diagnostics of the SCGD are performed in this work, including electrical measurements, electron densities and rotational and excitation temperatures. In particular, these measurements are performed introducing solutions with NaCl concentrations up to 3.5 g/L in order to understand how they affect the atomization/excitation efficiency and the analyte solution-to-plasma transfer processes of the source. The information is correlated with the signal produced by three analytes (Cd, Zn and Cu).

1. Introduction

Solution-electrode glow discharge plasmas are becoming a solid alternative as excitation sources coupled to Optical Emission Spectroscopy (OES) for elemental analysis [1]. In terms of analytical performance, its limits of detection (LODs) can compete with traditional elemental analysis techniques such as Atomic Absorption Spectrometry (AAS) or Inductively Coupled Plasma (ICP) with OES detection, showing mid to low ng/mL range for many elements, going even lower for some specific cases (e.g., Na, Li or Ag) [1]. Moreover, the detection of Cl and Br was recently reported, with LODs in the low μg/mL level [2]. The use of mass spectrometry (MS) detection improves some of these features and even extends the use of the source to analyze organic compounds and even large biomolecules [3,4].

One of these excitation sources is the Solution-Cathode Glow Discharge (SCGD). The SCGD is based on an electrical discharge at atmospheric pressure ignited and maintained with <100 W of direct current power with voltages normally below 1000 V, without requiring pressurized gases. Its special characteristic is the use of a conductive liquid electrode that is continuously renewed and electrically grounded, acting as the cathode; the anode is typically a pin metallic electrode a few mm above. In this situation, the plasma is continuously in contact with the solution, sampling it and incorporating the solution constituents into the plasma. In other words, there is no need to include a sample nebulization step to introduce it into the plasma and atomize it, providing a simple and low consuming OES source, with high miniaturization and portabilization potentials [5,6]. Once the atomized analytes are in the plasma, they eventually produce atomic emission useful for elemental detection and quantification, covering many elements in the periodic table, reaching many alkali, alkali-earth and transition metals, semi-metals and even halogens, especially if combined with hydride generation strategies [2,7–9]. Not in vain, SCGD-OES and similar set-ups were tested for the analysis of water of diverse provenance (lakes, rivers, tap or mineral) [10,11] and others with higher salinity content like seawater [6,11], waste waters [12,13], brines [14] or blood samples, [15] showing good tolerance to complex matrices with high concomitant ion concentrations [1]. Additionally, novel geometries (e.g., using hanging solution drop electrodes [16] or flat capillaries [17]) and powering modes (e.g., ms pulsed [18]) were reported attempting to improve the capabilities of the source. The overall

* Corresponding authors.
E-mail addresses: orejasjaime@uniovi.es (J. Orejas), pisonerojorge@uniovi.es (J. Pisonero).

https://doi.org/10.1016/j.sab.2023.106786
Received 21 July 2023; Received in revised form 7 September 2023; Accepted 10 September 2023
Available online 12 September 2023

characteristics of the SCGD indicate it can be a valuable approach for continuous real-time elemental monitoring in water streams analysis.

Nevertheless, the simplicity of this plasma to serve simultaneously as a nebulization/atomization/excitation source entails additional complexity. The mechanisms under which the plasma incorporates the elemental analytes and the excitation processes (that fortunately are better understood from the experience with other plasma excitation sources) are difficult to untangle. Analyte solution-to-plasma transfer occurs in a complex environment where liquid, gas and plasma phases coexist, generating an extremely rich chemical environment with the presence of many different reactive species (e.g., hydrated electrons or H and OH radicals). Additionally, the discharge presents a fast temporal fluctuation (in the low μs scale) not usual in metallic electrode discharges, adopting a filamentary structure. These plasma filaments prospect the liquid electrode surface in a somehow chaotic way [19,20]. Different mechanisms under which this solution-to-plasma analyte transfer were proposed. Cserfalvi and Mezei proposed cathodic sputtering by H_2O^+ and O^+ as a way of producing solvated metallic ions that can lead to neutral metal-hydroxide complexes capable of travelling across the strong electric field cathode region [21], of over 10^6 V/m [22]. Maksimov et al. proposed a similar cathode sputtering mechanism where neutral metallic species appear after the break of vibrationally excited salt molecules presenting a bond of covalent nature (instead of the typical non excited ionic bond nature) [23]. An alternative mechanism was proposed by Webb and coworkers, involving analyte containing droplets ejected from the solution surface, either generated by electrospraying or through flash thermal vaporization (rapid vaporization of a small volume of liquid that creates a high-pressure water vapor region that condensates and expels the droplets), followed by droplet desolvation and analyte release [24]. The droplet analyte transfer mechanism was later supported by other studies [19,20,25,26] and gained more weight under Hazel et al. work, where they introduced undigested nanoparticles and still found analyte emission [27]. Cathodic sputtering produced by impinging H_2O^+ ions, much less massive than nanoparticles, would require much higher ion kinetic energies to extract the nanoparticles from the liquid solution. On the contrary, the droplet ejection mechanism rationalizes the nanoparticle transfer, immersed in those droplets, from the solution into the plasma. Apart from cathodic sputtering and droplet ejection, a third mechanism was described, involving Chemical Vapor Generation (CVG) containing the analytes, through the reduction of the dissolved metals in the plasma-liquid interface. In this sense, SCGD set-ups were utilized as Plasma Induced CVG approaches to generate vapors of Hg [28] or Os [29], along with similar set-ups using alternate current discharges (Cd or Zn [30]) or solution-anode polarities (Ag, Cd, Hg, In, Pb, Tl and Zn [31]).

As it has been mentioned, the performance of SCGD and alike sources resist reasonably well if high non-analyte ion concentrations are present in the sample solution. Two of the most typically present ions in many target samples are Na^+ and Cl^-. Their effect on the analytical signal was studied for multiple analytes introducing prepared solutions with different amounts of Na^+ and Cl^- before dealing with real samples. The results for this response study are summed up in Table 1. Na^+ effect has been studied for more elements in concentrations up to the range of 100 s of mg/L, producing sensitivity drops for many elements, though some others did not show notable signal response changes. Attending to these exceptions, they are difficult to classify since some of them are alkali, other alkaline-earth and other transition metals. Cl^- did produce sensitivity changes in every analyte that has been studied, with generalized sensitivity drops, except for one element, Hg, which doubled its response.

For real sample analysis, where high concentrations of Na^+ and/or Cl^- are found, previous dilution step is typically reported. This procedure is a plausible option, but sometimes demands reaching high sensitivities to compensate from reducing the concentration of analyte ions, together with concomitant ions. In this sense, studying analyte response at concomitant ion concentrations similar to that of high salinity samples is desirable. Additionally, to our knowledge, no detailed study on how concomitant ion concentration affects the SCGD plasma conditions and its working mechanisms when used for elemental analysis (both solution-to-plasma analyte transport mechanisms and excitation processes) has been performed to date.

Table 1
Reported analytical signal variation in SCGD-OES due to the presence of concomitant ions.

Concomitant		Analyte	Signal Variation	Reference
Ion	Concentration (mg/L)	Element		
Na^+	200	Hg	No change	[12]
	100	Cs	No change	[32]
	100	Rb	No change	[32]
	100	Sr	No change	[32]
	200	Cd	No change	[33,34]
	5	Ca	Decrease	[15,35]
	100	Ca	Decrease	[35]
	100	K	Decrease	[14,35]
	200	K	Decrease	[14,35]
	200	Mg	No change	[14]
	200	Ag	Decrease	[34]
	200	Zn	Decrease	[34]
Cl^-	200	Hg	Doubled	[12]
	100	Cs	Decrease	[32]
	100	Rb	Decrease	[32]
	100	Sr	Decrease	[32]
	200	Cd	Decrease	[33,34]

The present study unveils how the presence of two common ions, Na^+ and Cl^-, present in many potential samples where the SCGD-OES approach can find a niche of applications, affects both the analyte transport and excitation mechanisms from fundamental plasma characterization experiments. This task is confronted by the characterization of the electrical parameters of the discharge and the measurement of relevant plasma parameters, namely, rotational temperature, electron density and excitation temperature, introducing solutions with increasing NaCl concentrations. These results are correlated with the signal produced by three analytes (Cd, Zn and Cu), with a discussion about the excitation conditions and the analyte transfer mechanisms of the SCGD and similar sources.

2. Experimental

2.1. SCGD-OES set-up

Fig. 1 schematizes the experimental set-up used in the experiments. The SCGD is generated between a sharpened tungsten rod and a graphite, covered by an electrolytic solution and connected to ground. A borosilicate glass capillary tubing of 1.1 and 0.4 mm of outer and inner diameter, respectively, leads the solution into the discharge region. The solution flow rate is controlled with a peristaltic pump (Reglo Icc, Ismatec, Wertheim, Germany). A tube section filled with glass beads helps to damp the flow rate pulsing produced by the pump. The solution flows continuously to assure no exposition of the graphite surface. A direct current high voltage power supply (KEPCO, Model BHK 2000–01, New York, USA) applies a potential difference between the two electrodes. The ignition is achieved by applying a potential difference of 1500 V and approaching the metallic electrode (a tungsten rod that acts as anode) to the overflowing electrolyte. Once ignited, the discharge is maintained at 80 mA (the power supply works in current control mode) which requires between 600 and 900 V, depending on the inter-electrode distance, which ranges between 1 and 4 mm, and the incoming solution composition. The applied discharge potential is measured using a high voltage probe (TESTEC, HVP-40). Direct voltage readings provide the voltage between the metallic electrode and the graphite, which includes the voltage applied to the discharge plus the voltage between the solution surface and the graphite. To estimate the

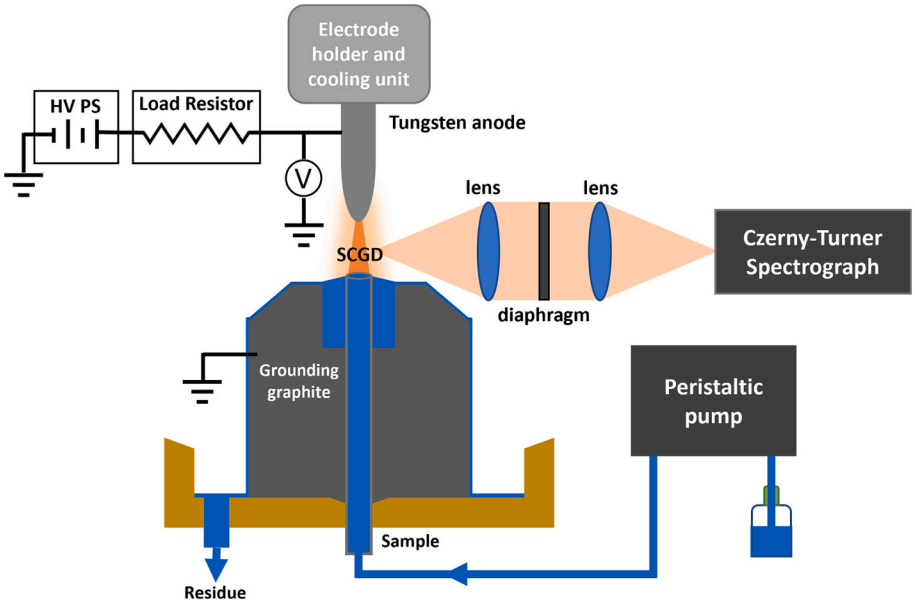

Fig. 1. Schematic presentation of the SCGD-OES set-up used in the present study.

real voltage applied to the discharge, the voltage between the solution surface and the grounding graphite needs to be subtracted to the one measured by the high voltage probe. The voltage between the solution surface and the graphite is measured using the same voltage probe, and by approaching the metallic electrode to the solution. Once the electrode is in slight contact with the solution, the power supply provides a current of 80 mA (without ignition) and the voltage between the metallic electrode and the graphite is measured with the high voltage probe. This measurement is performed with each solution at different NaCl concentrations, which impact the conductivity of the solution and this voltage with it. Each voltage measured while the discharge is on is then corrected removing the mentioned contribution with the respective value to obtain a better estimate of the discharge voltage. The specific solution voltage drop values are plot in Fig. S1 (Appendix).

A pair of fused silica lenses (50.8 mm diameter, 300 mm focal length, LB4710, Thorlabs) focus the optical emission generated by the plasma (magnification of 1:1) onto the entrance slit of a spectrograph (SpectraPro 2500i, Princeton Instruments, Inc., USA) equipped with two diffraction gratings of 2400 and 3600 grooves/mm. An intensified charge coupled device (ICCD) detects the optical emission for posterior data treatment (PI-MAX 1024RB, Princeton Instruments, Inc., USA). In between the lenses, a shutter diaphragm controls the throughput of the system and reduces potential spherical aberration. The diaphragm is used in the OH band and Cu lines measurements since the spherical aberrations are notable. No diaphragm is used for the H_β emission line (486.1 nm) since the spherical aberration is not noticed. The registered intensities are corrected according to the wavelength efficiency of the system, which was obtained by using calibrated deuterium and tungsten lamps to cover a spectral region from 200 to 700 nm. The lateral resolution provided by this imaging system is estimated using a 1951 USAF test target (Thorlabs, Germany). The target is back illuminated using a regular incandescent reading lamp at the SCGD position using the diffraction grating at zero order, hence working like a mirror, with the spectrograph slit totally open. The target stripes are considered resolved if separated at half of maximum intensity recorded in the image. According to this, the system can resolve 10 lines/mm, resulting in a spatial resolution of 100 μm. It is important to mention here that the resolution can change at different wavelengths due to changes in the refraction index of the lenses, especially in the UV. The value obtained here using a continuous source with its maximum in the visible range, probably worsens in the UV range. The spectroscopical measurements to be used in the calculations of certain plasma parameters (electron density, rotational temperature and excitation temperature) at different discharge heights are first taken without binning. In the post-treatment, the signal for each row of 5 pixels (corresponding to a discharge height of 125 μm) is accumulated to obtain each parameter (emission intensity, rotational temperature, electron density and excitation temperature) value per 125 μm section.

The raw data registered by the spectrograph software (WinSpec 32, Princeton Instruments, Inc., USA) were analyzed using Matlab for further data processing and/or OriginPro for graphic presentation.

2.2. Reagents and solutions

Every solution is prepared with deionized water (specific resistivity 18.2 MΩ·cm) and nitric acid (HNO_3, 68 wt%, Labkem) added to a final concentration of 0.1 M. Sodium chloride (NaCl, ≥99.5%, Sigma-Aldrich) is added to reach several concentrations (0.0000, 0.0035, 0.035, 0.35, 0.7, 1.75 and 3.5 g/L NaCl). Cu, Cd and Zn stock solutions are prepared in 0.1 M HNO_3 solution at a concentration of 1000 ng/mL out of the corresponding salts ($Cu(NO_3)_2{\cdot}3H_2O$, VWR Chemicals, $Cd(NO_3)_2{\cdot}4H_2O$, Alfa Aesar and $ZnCl_2$, Sigma-Aldrich). These stock solutions are added to the different NaCl concentration solutions to end with 1 μg/mL metal concentrations for analyte signal response measurements and 100 μg/mL Cu concentration for the excitation temperature measurements.

3. Results

3.1. Cathode voltage drop and positive plasma column electric field

The electrical characteristics of the discharge can be scrutinized to obtain information on the SCGD electric field in specific regions of the discharge. As in other glow discharges, the electric potential is not uniformly distributed along the whole plasma column: most of the potential drop is concentrated in areas close to the cathode, and a secondary contribution is found in the positive column, which increases linearly with the inter-electrode distance, since the electric field in this area is almost constant [32]. At atmospheric pressure, most of the volume is covered by the positive column and, if the interelectrode distance is increased, only this region extends its length. Consequently, the potential increases proportionally with the inter-electrode distance. Thanks to this fact, Cserfalvi et al. proposed a method to estimate the

cathode voltage drop and the electric field in the positive column [33]. Briefly, by measuring the voltage applied to the discharge at different inter-electrode distances, a linear extrapolation to a hypothetical distance of zero provides an estimation of the cathode voltage drop, while the slope of the curve provides the electric field in the positive column.

Fig. 2(a) and (b) show the results of the voltage (once the contribution of the solution is removed, as explained in the experimental section) vs interelectrode distance measurements with the corresponding linear fittings, and the results for the cathode voltage drops and the positive column electric fields, at increasing NaCl concentrations, respectively. Error bars in Fig. 2(b) were estimated from constant and slope errors obtained in the corresponding linear fittings. In general, the voltage at every inter-electrode distance decreases as the NaCl concentration increases (see Fig. 2(a). Attending to Fig. 2(b), the cathode voltage drop stays constant up to 0.7 g/L NaCl, with a decrease above that concentration after which the voltage stays constant again. Despite this behavior, the reduction is minor (barely 11 V, around 2% reduction when comparing the maximum NaCl concentration and the case without added salt). In any case, the overall values agree well with previous measurements [20,33]. For the positive column electric field, the decrease is noticeable from 0.35 g/L onwards, with further reduction at higher NaCl concentrations. In this case, the electric field reduction reaches around 16% at 3.5 g/L NaCl, again compared with the case without salt.

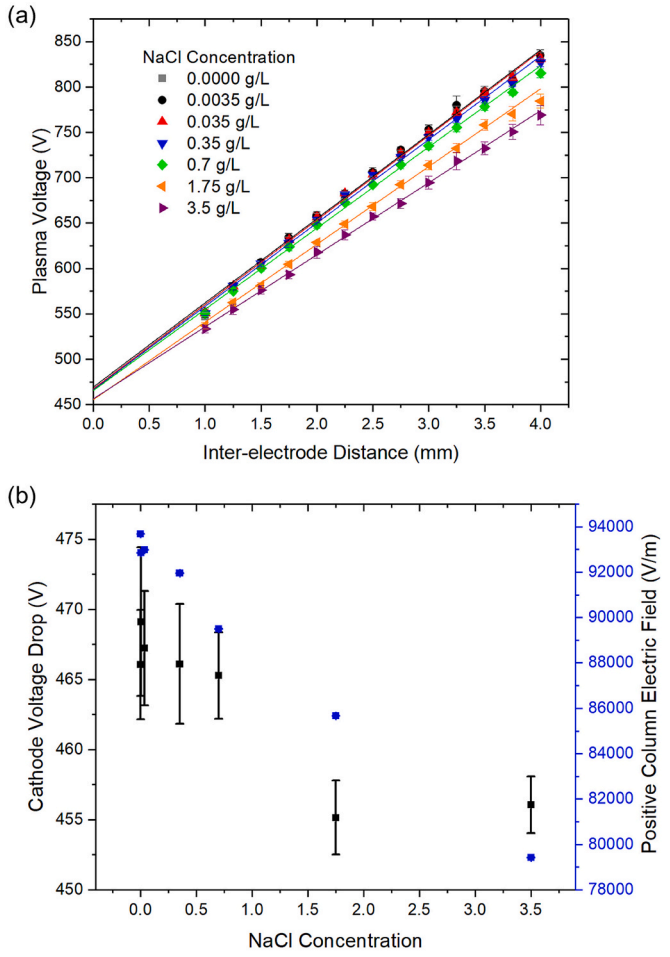

Fig. 2. a) Plasma voltage vs Interelectrode distance, including the fitted lines and b) cathode voltage drop and positive column electric field at different NaCl concentrations. Error bars were estimated from constant and slope errors obtained in the corresponding linear fittings.

3.2. OH rotational temperature with spatial resolution

OH rotational temperature is measured using the Izarra method [34]. Shortly, the method requires to measure the peak intensity ratio of two unresolved groups of lines (situated at 306.5 and 306.8 nm, and designated as G_0 and G_1, respectively, in reference [34]) over another reference group of lines (309.0 nm, designated as G_{Ref}), all of them corresponding to the rotational fine structure of electronic vibrational transition OH molecule, $A^2\Sigma$ ($v' = 0$) ➔$X^2\Pi$ ($v'' = 0$). An example of the resulting spectral images is included as supplementary information, Fig. S2 (Appendix). The ratio between the intensities of these lines depends on how populated the respective rotational states in the vibrational $v' = 0$ level of the $A^2\Sigma$ electric state of the molecule are. The population of the upper levels of the first two groups of transitions, have certain dependence on the temperature, while the upper levels of the third one are readily populated at low temperatures and their resulting intensity barely depends on the temperature. Although the resulting rotational temperature cannot be directly recognized as the gas temperature (the rotational distribution might be characterized by more than one temperature due to different production pathways of the excited OH states ($A^2\Sigma$) [35]), it can still provide information about possible changes in the plasma excitation capabilities. Once the instrumental linewidth of the optical set-up is determined (0.04 nm, using a slit width of 85 μm), intensity ratios are compared with the ones tabulated at specific rotational temperatures in the range of 600–8000 K for that same instrumental linewidth [34]. This method is applied to the measurements of OH unresolved intensity ratios at different discharge heights (e.g., at different ICCD pixel rows) to obtain spatially resolved values of the rotational temperature. The raw intensities are corrected according to wavelength and pixel-to-pixel efficiency. A homemade Matlab program processes the raw data, providing a temperature value every 125 μm of discharge height. More details about the implementation of the method are included as supplementary information.

Fig. 3(a) shows the spatially resolved rotational temperature results using the G_0 over G_{Ref} and G_1 over G_{Ref} intensity ratios mean value, at different NaCl concentrations. Fig. 3(b) shows the rotational temperature versus NaCl concentration at 0.4 mm, 1.4 mm and 2.0 mm distance from the anode (cathode situated at 2 mm). Fig. S3 (Appendix) in supplementary material shows the spatial distribution of the OH emission at the G_0, G_1 and G_{Ref} wavelengths, which are used in the calculations of the rotational temperatures.

Three regions with different behavior versus NaCl concentration can be identified. In the first region (0.0–0.8 mm), the rotational temperature descends at increasing NaCl concentration. In the second region (0.8–1.9 mm), it barely changes up to a concentration 0.7 g/L NaCl. However, higher concentrations increase the rotational temperature in this region. The third region (~2.0 mm), close to the cathode, follows a similar trend to the first region, though at a lower overall temperature.

3.3. Electron density with spatial resolution

The presence of high quantities of Na^+ or Cl^- in the plasma can change the excitation conditions inside the plasma. In this sense, the electron density and the excitation temperature can suffer variations that could eventually explain a lower analyte emission rate. For this reason, the electron density is also estimated with spatial resolution. In this case, the electron density is obtained from the H_β Stark broadening effect, making use of the Gigosos-Cardenoso model [36], which covers electron densities between 10^{14} and 10^{19} cm^{-3} and electron temperatures between 10^3 and 10^6 K. Previous measurements indicate that these ranges of conditions are fulfilled by the SCGD plasma [15,37,38]. More in detail, the H_β linewidth is related with the electron density with the following expression [36]:

$$\Delta\lambda\ (\mathrm{nm}) = 4.800 \cdot \left(\frac{N_e\ (\mathrm{cm}^{-3})}{10^{17}}\right)^{0.68116}$$

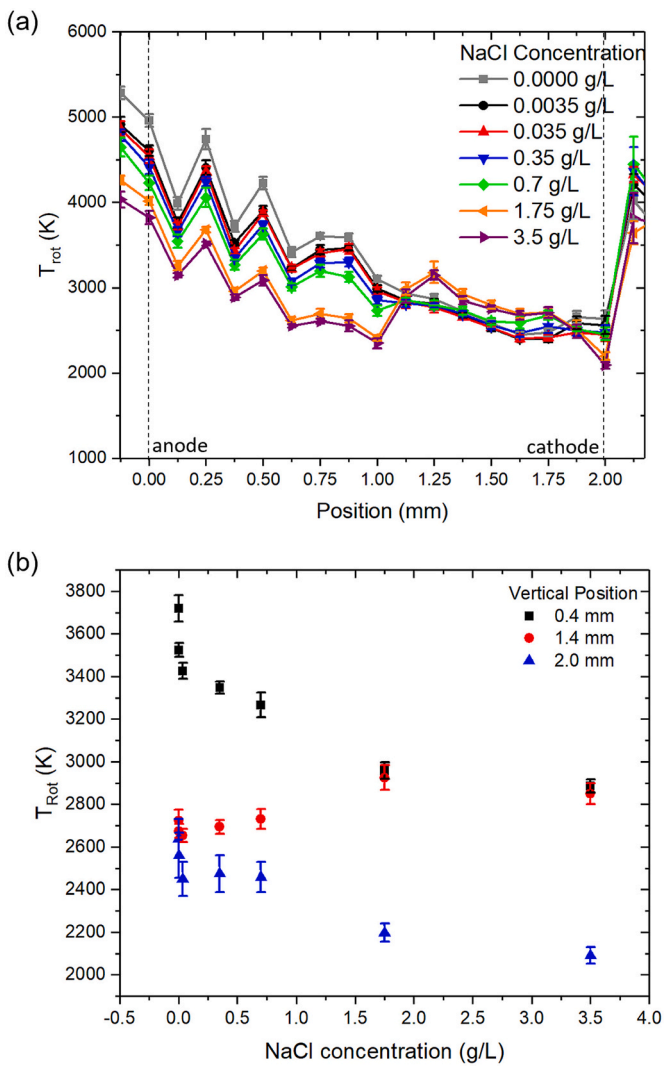

Fig. 3. a) Spatially resolved OH rotational temperature along the SCGD column b) OH rotational temperature at specific positions along the SCGD column introducing variable NaCl solutions. Error calculations are detailed in supplementary information (Appendix).

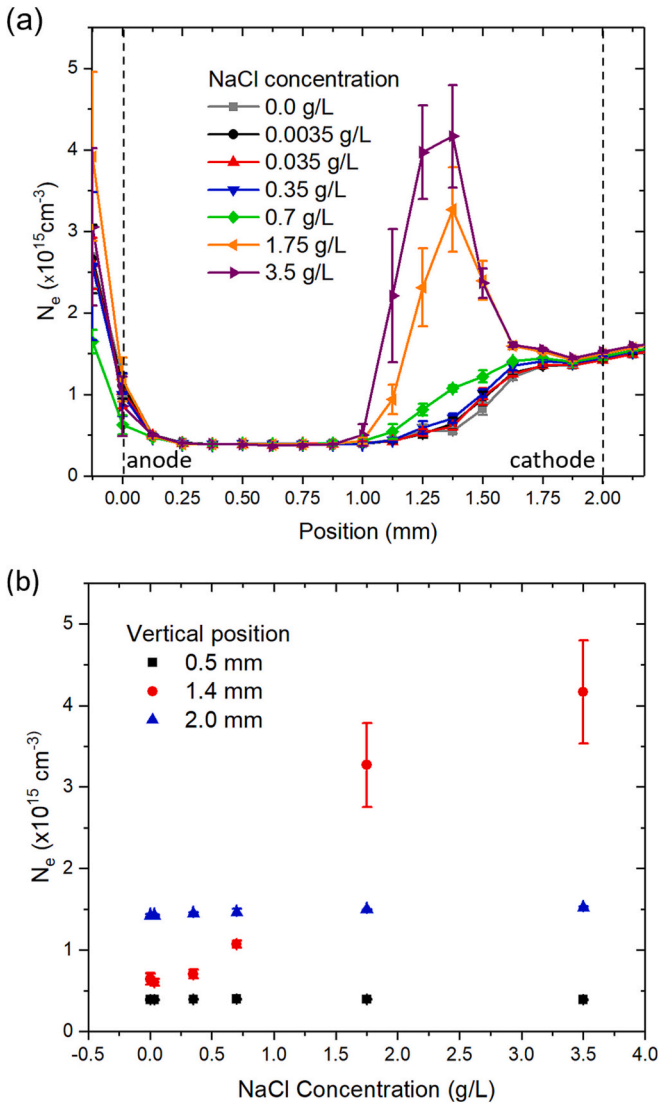

Fig. 4. a) Spatially resolved electron density along the SCGD column b) electron density at specific positions obtained introducing variable NaCl concentration solutions. Error calculations is detailed in supplementary information (Appendix).

being $\Delta\lambda$ the line width and N_e the electron density. Spatially resolved values of the electron density are also calculated every 125 μm of discharge height. Raw data are processed using a homemade Matlab program. Fig. S5 (Appendix) in supplementary information shows an example of a spectral image and three spectra at different heights, including a brief description of the data treatment process.

Fig. 4 shows the electron density behavior at different height in the plasma, at several NaCl concentrations. No notable change is observed from 0.0 to 1.0 mm distance from the anode for the whole NaCl concentration range. From 1.0 to 2.0 mm, there is a slight increase in the electron density up to 0.7 g/L of NaCl. At this concentration, the increase is more notable in the electron density, especially in the region between 1.0 and 1.6 mm, with a maximum value at 1.4 mm. Interestingly, the electron density increase is also noticed by the red shift that the H_β emission line suffers (included as supplementary information in Fig. S6 (a) (Appendix)), albeit noticeable at a lesser degree. The electron density increase is quite likely produced by the presence of high amounts of Na inside the plasma and its low ionization potential. Thus, Na is highly susceptible to be ionized, supplying the plasma with extra electrons. Though Cl transferred into the plasma could have an impact here, Tachibana and Yasuoka reported the low transfer efficiency of dissolved Cl^- into the plasma for a similar device, so its contribution is likely to be negligible [39]. Interestingly, the electron density increase is localized at the end of the positive column (see Fig. S7 (Appendix) for a total emission image of the SCGD) where electrons gain enough energy from the electric field to efficiently ionize the Na atoms present in the plasma. This localized electron density rise appears at the end of the positive column closest to the cathode, right before the brightest region of the plasma, which corresponds to several regions, including the negative and cathodic glows. This result explains the notable decrease of the positive column electric field (of roughly 16%) and a much smaller change in the cathode voltage drop (of 2%) (see Fig. 2(b), at the highest NaCl concentrations assayed: more electrons mean more charge carriers, that require less voltage to reach the same current (e.g., power supply works in current control mode). Also interestingly, OH rotational temperature changes in this same region at 1.75 g/L NaCl (see Fig. 3). Additionally, the spatial distribution of Na emission at 589.0 nm (included in Fig. S6(b) (Appendix) shows new emission maximum in this same region: up to 0.7 g/L NaCl, though present in the whole discharge column, Na emission, presents an important peak around 1.6–1.7 mm, which roughly corresponds to the end of the positive column, just above

the cathode region, depending on the Na concentration (see Fig. 4(b)). Over 0.7 g/L NaCl, Na excitation is also prominent along the whole positive column and close to the metallic anode. This change in the spatial emission distribution shows that the excitation conditions are changed and can affect the sensitivity for targeted analytes.

3.4. Excitation temperature with spatial resolution

Emission lines in the SCGD plasma do not have a spatially uniform distribution. Moreover, the changes in the electron density and Na emission spatial distribution suggest that modifications of the emission line spatial pattern can arise from the NaCl content of the incoming solution. Fig. 5 (a), (b) and (c) show the intensity spatial profile of Cu emission lines at 324.7 nm (resonant line), 510.6 nm and 521.8 nm, respectively, introducing a solution with 100 μg/mL Cu^{2+} at different NaCl concentrations. Despite the differences in the energies of the Cu upper levels involved (3.8 and 6.2 eV, see Table 2), the changes are similar in the three cases: at low NaCl concentration, the emission spreads along the whole plasma column, with a maximum in areas close to the cathode; over 0.7 g/L NaCl, the emission close to the cathode depresses, while in areas closer to the anode, the signal slightly increases.

From the measurement of atomic emission line intensities with spatial resolution, the plasma excitation capability can be evaluated. The optical emission of Cu, which is contained in the incoming solution, allows to obtain the excitation temperature in the discharge with spatial resolution. The excitation temperature is calculated from a Boltzmann plot obtained with Cu emission intensities measured in the spectra resulting from the 5-row grouping. Table 2 shows the spectroscopic parameters of the emission lines included in the calculations obtained from the NIST Atomic Database [40]. It is important to highlight here that some other Cu emission lines are not included due to spectral interferences produced by Na emission lines coming from the high NaCl concentrations used in some of the solutions. Fig. S8 (Appendix) shows some of the resulting Boltzmann plots obtained at four different positions along the plasma column, at three NaCl concentrations.

Fig. 6 shows the results for the Cu excitation temperature spatial resolution, respectively, at different NaCl concentrations. In areas close to the anode and at 2.0 mm (right at the solution surface) the uncertainties of the measurements are notably higher. First, Cu intensities for some lines in this area are low, especially at high NaCl concentration. And second, the solution surface is quite chaotic [20], so the stability of the emission is concerned. These two aspects hamper the linear fittings and the excitation temperature measurements. In the region between 0.4 and 1.9 mm, the excitation temperature presents little variation up to 0.7 g/L NaCl. There is, however, a small reduction of roughly 10% at the highest NaCl concentrations (1.75 and 3.5 g/L NaCl) localized in the region between 1.0 mm and 1.9 mm, right where the atomic emission depresses (see Fig. 5).

3.5. Analyte signal behavior and mechanistic insights

Fig. 7 (a) shows how Zn I, Cd I and Cu I net signals (integrated at 213.8, 228.8 and 324.7 nm, respectively), behave at different NaCl concentrations, and Fig. 7(b) presents their signal-to-noise (S/N) and signal-to-background (S/B) ratios. Every analyte concentration is 1 μg/mL. Net intensity suffers little variation up to NaCl concentrations of 350 mg/L (corresponding to ~140 mg/L of Na^+ and ~210 mg/L of Cl^-). Above this concentration, signal suppression appears, being more pronounced for Cu than for Cd or Zn. Moreover, S/N and S/B present an analogous behavior. Nevertheless, S/B seems to decrease less, as compared to the net signal or the S/N, since the background emission decreases at increasing NaCl concentrations [41], while the noise is somehow maintained. In any case, though the matrix effects are present, they are not a serious limitation for the analysis and shows the robustness of the SCGD against high NaCl content samples. Webb et al.

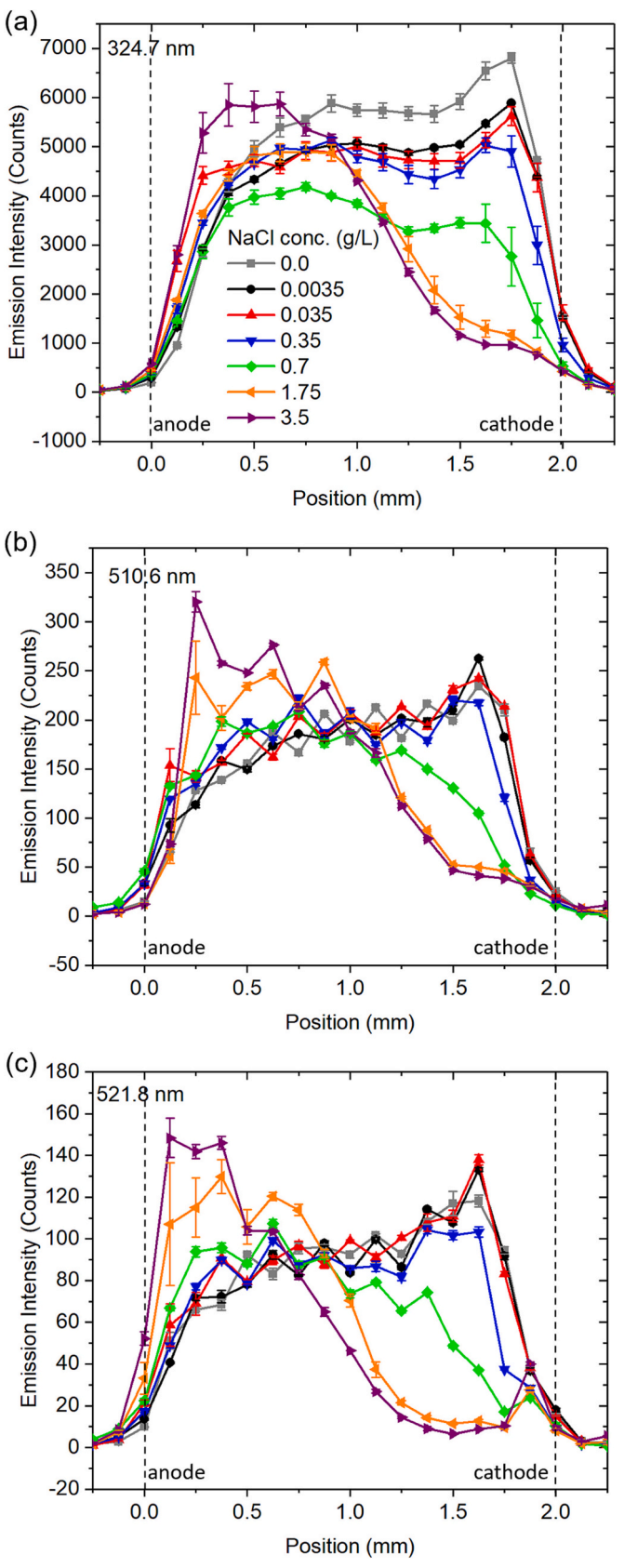

Fig. 5. Spatially resolved Cu emission introducing a solution containing 100 μg/mL of Cu and increasing concentrations of NaCl at the following wavelengths: a) 324.7 nm; b) 510.6 nm; c) 521.8 nm. Errors are calculated from the standard deviation of five measurements.

Table 2
Cu I emission lines included in the Boltzmann plots, including the energies and configurations of the levels involved in the transition and the transition probabilities (A_{ki}).

λ (nm)	Lower Level		Upper Level		A_{ik} (s^{-1})
	Energy (eV)	Conf., Term and J value	Energy (eV)	Conf., Term and J value	
402.3	3.79	$3d^{10}4p\ ^2P^0\ 1/2$	6.87	$3d^{10}5d\ ^2D\ 3/2$	$1.90{\cdot}10^7$
406.3	3.82	$3d^{10}4p\ ^2P^0\ 3/2$	6.87	$3d^{10}5d\ ^2D\ 5/2$	$2.10{\cdot}10^7$
510.6	1.38	$3d^9 4s^2\ ^2D\ 3/2$	3.82	$3d^{10}4p\ ^2P^0\ 3/2$	$2.00{\cdot}10^6$
521.8	3.81	$3d^{10}4p\ ^2P^0\ 3/2$	6.19	$3d^{10}4d\ ^2D\ 5/2$	$7.50{\cdot}10^7$
578.2	1.64	$3d^9 4s^2\ ^2D\ 3/2$	3.78	$3d^{10}4p\ ^2P^0\ 1/2$	$1.65{\cdot}10^6$

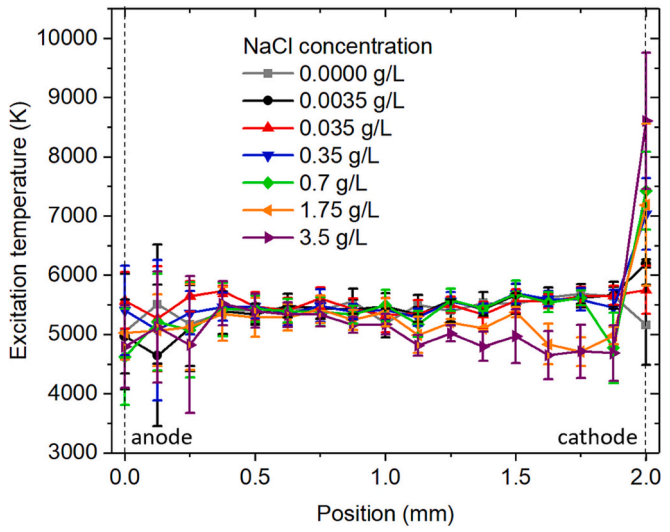

Fig. 6. Spatially resolved Cu excitation temperatures at different NaCl concentrations. Error bars were obtained propagating the error obtained from the linear fitting of the corresponding Boltzmann plot.

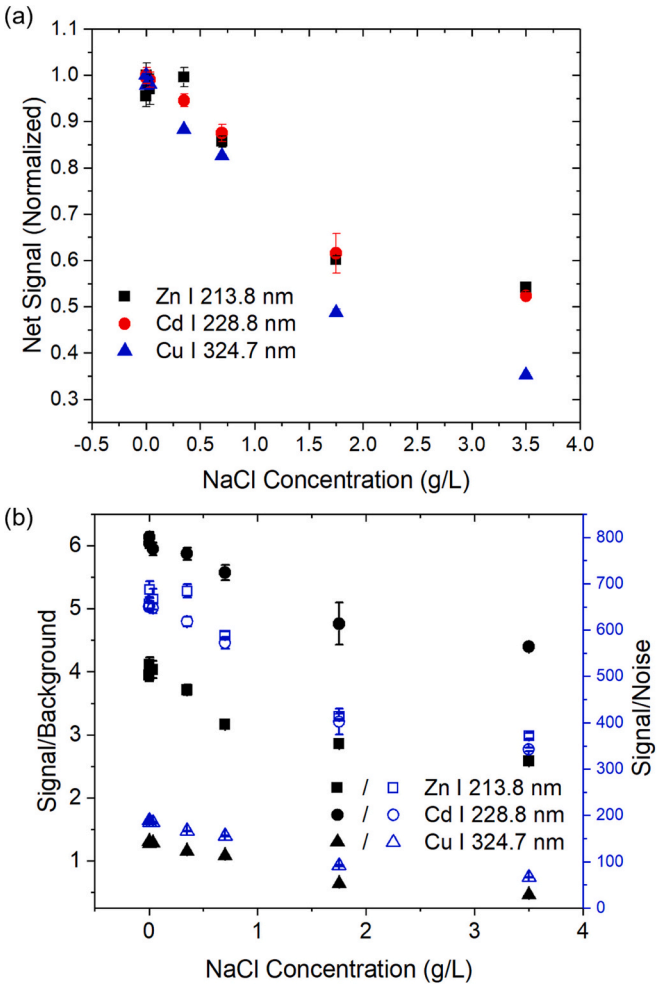

Fig. 7. a) Net signal (net signal errors are obtained from the standard deviation of five measurements.) and b) S/B and S/N for Zn, Cd and Cu at increasing NaCl concentration. Error bars have been calculated by propagating the net signal errors.

performed similar measurements, showing stronger drops in Cd and Cu net signals (background subtracted) of around 70% at 25 mM of Na^+, versus the 40–50% signal drop at 1.75 g/L NaCl (roughly 30 mM Na^+) observed in this study. While the change is noticeable, they both fall in similar ranges and can be addressed by differences in the discharge and optical set-ups [24].

Comparing these results with the ones provided in previous sections, the 0.7 g/L NaCl concentration seems to be an inflexion point for the behavior of different parameters, and analyte net signals are not an exception. In terms of the excitation conditions, despite the increase in the electron density, the excitation temperature falls slightly in a quite specific region of the plasma. Thus, it can be considered that the excitation conditions are deteriorated, partially explaining the loss in sensitivity due to a slight reduction of electron energy. Therefore, electrons loose efficiency in exciting atoms, despite their increase in number density. These results are similar to those reported by Webb et al., considering that spatially averaged data is provided there [24]. The decreasing tendency in the cathode voltage drop and positive column electric field can explain the loss in the electron energies: lower cathode voltage drop and, especially, from the positive column electric field values (see Fig. 2) obtained at those conditions suggest that electrons are accelerated less.

In terms of analyte behavior, there is a reduction in the Cu excitation temperature, which does not exceed 10%. Additionally, Cd I 228.8 nm and Zn I 213.8 nm suffer a lesser decrease in their net signal values, compared to Cu. Their corresponding transition excited states are situated at 5.4 and 5.8 eV, while Cu I 324.7 nm is situated at 3.8 eV. In this sense, a stronger signal depression would be expected for Cd or Zn. Therefore, the solution-to-plasma transport efficiency might be affected as well. This change in the transport efficiency was envisaged by Webb and coworkers, reporting that analyte concentration was notably diminished when Na^+ concentration in the incoming solution reached 1000 ppm, and explaining it suggesting a less efficient droplet formation and desolvation process [24].

Within the described mechanisms for analyte transport, two of them are related with the cathode voltage drop variation: cathodic sputtering and electrospray-based ejection of droplets; on the contrary, droplet ejection through fast thermal vaporization and CVG are less dependent on it. Cathodic sputtering relies on the strong electric field in the cathode area that accelerates impinging ions that eventually release analytes from the solution into the plasma. Given that the cathode voltage drop does not change drastically (see Fig. 2), it is quite likely that the electric field close to the cathode remains almost the same. In that sense, it seems unlikely that the presence of NaCl contribute to a change in the analyte transfer through this mechanism and cannot explain the loss of analyte signal. Similarly, electrospray ejected droplets require a strong electric field at the liquid surface to generate Taylor cones and produce matter ejection. Given that little change in the cathode voltage drop is found, the electric field in areas close to the solution surface should not change either. Nevertheless, the presence of NaCl in solution is also relevant in the surface tension of the solution. Surface tension is increased due to a stronger interaction between water molecules and dissolved ions, compared to the interaction between water molecules. Nevertheless,

surface tension presents a minimum around 0.06 g/L of NaCl [42]. In electrosprays, a larger surface tension usually increases the required voltage to release solution droplets from a formed Taylor cone (Voltage$\propto$ (surface tension)$^{1/2}$) [43]. However, the maximum relative increase for the surface tension is small, of about 0.3% at around 6 g/L [42]. It seems that these changes are not likely to be important in the formation of Taylor cones and droplet ejection and, consequently, to the observed signal drop. The alternative droplet ejection mechanism, the thermally based one, is related with the gas temperature of the plasma at the liquid surface. The measured rotational temperatures are quite likely providing temperatures above the gas temperature and are not reliable to be analyzed as such. But the detected changes in the rotational temperature above the solution surface suggest that the presence of NaCl in solution generates changes in the excitation mechanisms of OH.

Though the CVG mechanism for solution-to-plasma analyte transport cannot be directly studied from the experimental results shown here, there is one aspect that can be highlighted. When comparing the SCGD and similar set-ups using solution-anode polarities, matrix effects are more important and signal response is more element dependent in the latter [1]. Additionally, solution-anode polarities do not generate droplet ejection, and the sputtering is expected to be much less important (the main bombarding species are electrons), so the main analyte transport mechanism is CVG. In this sense, the SCGD probably has better resistance to the presence of ions due to the coexistence of more varied solution-to-plasma analyte transport mechanisms (cathode sputtering and droplet ejection) that, from the results presented here, are probably less affected by the presence of high concomitant ion concentration. Furthermore, the element dependency of the signal reduction observed in Fig. 7 (signal depression is stronger for Cu than Cd or Zn) can be explain considering CVG. CVG has a strong element dependency, since its efficiency is affected by the reduction potential of the corresponding cation and the specific volatile species that is formed (e.g., Cd and Zn can form gas phase hydrides). Also, Cd and Zn are more prone to CVG than Cu. In this sense, if the reduction capacity of the plasma-liquid interface is diminished, Cu is expected to be more affected than Cd or Zn. On the contrary, cathode sputtering and droplet ejection are less element dependent, since are purely physical mechanisms. If they were diminished due to the presence of NaCl, every element response should be decreased similarly.

In terms of the analyte solution-to-plasma transfer rate, it seems that it should not be affected by the electron density change, as its rise is localized in a region where the transfer does not take place.

4. Conclusions

Though the SCGD-OES technique has shown a robust performance in the presence of Na^+ and Cl^- in many publications, above certain concentration levels the signal of many elements tends to decrease. From the results shown here, the signal suppression can be generated by a mixture of the deterioration of the analyte solution-to-plasma transfer rate and the excitation conditions inside the plasma.

The cathode voltage drops slightly at high NaCl concentration and, therefore, the electric field in regions close to the solution cathode surface presents minor changes that seem insufficient to affect cathodic sputtering or electrospray-based droplet ejection (the latter seems not affected either by the change in the surface tension due to the presence of the salt). Rotational temperature presents a slight increase in regions close to the end of the positive column, right above the cathode region at high NaCl concentration, while showing a slight decrease close to the cathode surface. Electron density measurements do not show significant changes but when the NaCl concentration goes over 0.7 g/L. At this point, the electron density is increased at the end of the positive column, just above the cathode region, supplied by the ionization of Na atoms. Nevertheless, electron energies in this region quite likely decrease, from the results of the excitation temperature, which is slightly reduced.

From these results, it seems that cathodic sputtering and electrospray droplet ejection mechanisms for analyte solution-to-plasma transport process are not hampered due to the NaCl content in solution, so the deterioration of excitation conditions could explain the loss in sensitivity. Nevertheless, the differences between the three elements included in this study (Zn, Cd and Cu) are difficult to explain from the changes in the excitation conditions. In this sense, the solution-to-plasma analyte transfer mechanism seems to be element dependent. Droplet ejection or cathodic sputtering mechanisms should not show differences in the element response. Another mechanism, CVG, related with the formation of volatile compounds through the reduction of dissolved ions, fits well with the element dependency. In any case, further experiments are required to provide more information about this mechanism and its element dependency, along with studies on droplet formation with different incoming solutions.

CRediT authorship contribution statement

Jaime Orejas: Conceptualization, Data curation, Formal analysis, Investigation, Supervision, Visualization, Writing – original draft, Writing – review & editing, Funding acquisition, Project administration. **Yinchenxi Zhang:** Data curation, Formal analysis, Investigation, Writing – review & editing. **Cristian Soto-Gancedo:** Data curation, Formal analysis, Investigation, Writing – review & editing. **Luis Javier Fernández-Menéndez:** Formal analysis, Software, Writing – review & editing. **Jorge Pisonero:** Supervision, Writing – review & editing, Funding acquisition, Project administration. **Nerea Bordel:** Supervision, Writing – review & editing, Funding acquisition, Project administration.

Declaration of Competing Interest

The authors declare that they have no conflict of interests of any kind.

Data availability

Data will be made available on request.

Acknowledgments

The authors acknowledge funding from project MCI-21-PID2020-113951GB-I00 and project MCINN-22-TED2021-131619B-I00, funded by the Spanish Ministerio de Ciencia e Innovación and the Agencia Estatal de Investigación. Yinchenxi Zhang appreciates the fellowship support from the China Scholarship Council.

Appendix A. Supplementary data

Supplementary data to this article can be found online at https://doi.org/10.1016/j.sab.2023.106786.

References

[1] P. Pohl, P. Jamroz, K. Greda, M. Gorska, A. Dzimitrowicz, M. Welna, A. Szymczycha-Madeja, Five years of innovations in development of glow discharges generated in contact with liquids for spectrochemical elemental analysis by optical emission spectrometry, Anal Chim Acta (2021) 338399, https://doi.org/10.1016/j.aca.2021.338399.

[2] M. Gorska, P. Pohl, Application of atmospheric pressure glow discharge generated in contact with liquids for determination of chloride and bromide in water and juice samples by optical emission spectrometry, Talanta. 237 (2022) 122921, https://doi.org/10.1016/j.talanta.2021.122921.

[3] A.J. Schwartz, K.L. Williams, G.M. Hieftje, J.T. Shelley, Atmospheric-pressure solution-cathode glow discharge: a versatile ion source for atomic and molecular mass spectrometry, Anal. Chim. Acta 950 (2017) 119–128, https://doi.org/10.1016/j.aca.2016.10.045.

[4] A.J. Schwartz, J.T. Shelley, C.L. Walton, K.L. Williams, G.M. Hieftje, Atmospheric-pressure ionization and fragmentation of peptides by solution-cathode glow discharge, Chem. Sci. 7 (2016) 6440–6449, https://doi.org/10.1039/c6sc02032a.

[5] W. Zu, Y. Wang, X. Yang, C. Liu, A portable solution cathode glow discharge-atomic emission spectrometer for the rapid determination of thallium in water samples, Talanta. 173 (2017) 88–93, https://doi.org/10.1016/j.talanta.2017.05.073.
[6] X. Peng, X. Guo, F. Ge, Z. Wang, Battery-operated portable high-throughput solution cathode glow discharge optical emission spectrometry for environmental metal detection, J. Anal. At. Spectrom. 34 (2019) 394–400, https://doi.org/10.1039/c8ja00369f.
[7] C. Huang, Q. Li, J. Mo, Z. Wang, Ultratrace determination of tin, germanium, and selenium by hydride generation coupled with a novel solution-cathode glow discharge-atomic emission spectrometry method, Anal. Chem. 88 (2016) 11559–11567, https://doi.org/10.1021/acs.analchem.6b02807.
[8] K. Greda, P. Jamroz, D. Jedryczko, P. Pohl, On the coupling of hydride generation with atmospheric pressure glow discharge in contact with the flowing liquid cathode for the determination of arsenic, antimony and selenium with optical emission spectrometry, Talanta. 137 (2015) 11–17, https://doi.org/10.1016/j.talanta.2014.11.073.
[9] M. Gorska, P. Pohl, Coupling of chemical vapor generation with atmospheric pressure glow discharge optical emission spectrometry generated in contact with flowing liquid electrodes for determination of Br in water samples, Microchem. J. 178 (2022), https://doi.org/10.1016/j.microc.2022.107391.
[10] J. Yu, Y. Kang, Q. Lu, H. Luo, Z. Lu, L. Cui, J. Li, Improvement of analytical performance of liquid cathode glow discharge for the determination of bismuth using formic acid as a matrix modifier, Microchem. J. 159 (2020), https://doi.org/10.1016/j.microc.2020.105507.
[11] J. Yu, S. Yang, D. Sun, Q. Lu, J. Zheng, X. Zhang, X. Wang, Simultaneously determination of multi metal elements in water samples by liquid cathode glow discharge-atomic emission spectrometry, Microchem. J. 128 (2016) 325–330, https://doi.org/10.1016/j.microc.2016.05.019.
[12] J. Yu, L. Yin, Q. Lu, F. Feng, Y. Kang, H. Luo, Highly sensitive determination of mercury by improved liquid cathode glow discharge with the addition of chemical modifiers, Anal. Chim. Acta 1131 (2020) 25–34, https://doi.org/10.1016/j.aca.2020.07.050.
[13] H. Li, W. Zu, F. Liu, Y. Wang, Y. Yang, X. Yang, C. Liu, Determination of gallium in water samples by atomic emission spectrometry based on solution cathode glow discharge, Spectrochim Acta Part B At Spectrosc. 152 (2019) 25–29, https://doi.org/10.1016/j.sab.2018.12.004.
[14] C. Yang, L. Wang, Z. Zhu, L. Jin, H. Zheng, N.S. Belshaw, S. Hu, Evaluation of flow injection-solution cathode glow discharge-atomic emission spectrometry for the determination of major elements in brines, Talanta. 155 (2016) 314–320, https://doi.org/10.1016/j.talanta.2016.04.060.
[15] J. Yu, X. Zhang, Q. Lu, X. Wang, D. Sun, Y. Wang, W. Yang, Determination of calcium and zinc in gluconates oral solution and blood samples by liquid cathode glow discharge-atomic emission spectrometry, Talanta. 175 (2017) 150–157, https://doi.org/10.1016/j.talanta.2017.07.040.
[16] K. Swiderski, K. Greda, P. Pohl, P. Jamroz, The sensitive determination of Ag, Pb and Tl as well as reduction of spectral interferences in a hanging drop cathode atmospheric pressure glow discharge excitation microsource equipped with a Dove prism system, J. Anal. At. Spectrom. 37 (2022) 517–527, https://doi.org/10.1039/d1ja00433f.
[17] N. Hazel, J. Orejas, S. Ray, A novel solution cathode glow discharge geometry for improved coupling to optical emission spectrometry, J. Anal. At. Spectrom. (2022), https://doi.org/10.1039/d2ja00063f.
[18] P. Zheng, Y. Yang, J. Wang, H.I.A. Qazi, M. Wu, Y. He, Q. Hu, N. Ding, Development of milli-second pulsed atmospheric pressure solution cathode glow discharge optical emission spectroscopy for detecting metal elements in aqueous solution, J. Anal. At. Spectrom. 37 (2022) 1806–1814, https://doi.org/10.1039/d2ja00122e.
[19] A.J. Schwartz, S.J. Ray, E. Elish, A.P. Storey, A.A. Rubinshtein, G.C.Y. Chan, K. P. Pfeuffer, G.M. Hieftje, Visual observations of an atmospheric-pressure solution-cathode glow discharge, Talanta. 102 (2012) 26–33, https://doi.org/10.1016/j.talanta.2012.07.096.
[20] J. Orejas, N. Hazel, S.J. Ray, The solution-cathode glow discharge in slow motion: characterization of glow discharge filament structure and droplet ejection using a rectangular capillary, Spectrochim Acta Part B At Spectrosc. 181 (2021) 106209, https://doi.org/10.1016/j.sab.2021.106209.
[21] T. Cserfalvi, P. Mezei, Investigations on the element dependency of sputtering process in the electrolyte cathode atmospheric discharge, J. Anal. At. Spectrom. 20 (2005) 939–944, https://doi.org/10.1039/b504610f.
[22] P. Mezei, T. Cserfalvi, The investigation of an abnormal electrolyte cathode atmospheric glow discharge (ELCAD), J. Phys. D. Appl. Phys. 39 (2006) 2534–2539, https://doi.org/10.1088/0022-3727/39/12/010.
[23] A.I. Maksimov, V.A. Titov, A.V. Khlyustova, Electrolyte-as-cathode glow discharge emission and the processes of solution-to-plasma transport of neutral and charged species, High Energy Chem. 38 (2004) 196–199, https://doi.org/10.1023/B:HIEC.0000027659.13545.fb.
[24] M.R. Webb, F.J. Andrade, G.M. Hieftje, Use of electrolyte cathode glow discharge (ELCAD) for the analysis of complex mixtures, J. Anal. At. Spectrom. 22 (2007) 766–774, https://doi.org/10.1039/b616989a.
[25] D.E. Moon, M.R. Webb, Imaging studies of emission and laser scattering from a solution-cathode glow discharge, J. Anal. At. Spectrom. 35 (2020) 1859–1867, https://doi.org/10.1039/d0ja00134a.
[26] N. Shirai, G. Suga, K. Sasaki, Mechanism of droplet generation and optical emission of metal atoms in atmospheric-pressure dc glow discharge employing liquid cathode, Plasma Sources Sci. Technol. 29 (2020), https://doi.org/10.1088/1361-6595/ab6abc.
[27] N. Hazel, J. Orejas, S.J. Ray, Evaluation of solution-cathode glow discharge atomic emission spectrometry for the analysis of nanoparticle containing solutions, Spectrochim Acta Part B At Spectrosc. 176 (2021) 106040, https://doi.org/10.1016/j.sab.2020.106040.
[28] Z. Zhu, G.C.Y. Chan, S.J. Ray, X. Zhang, G.M. Hieftje, Use of a solution cathode glow discharge for cold vapor generation of mercury with determination by ICP-atomic emission spectrometry, Anal. Chem. 80 (2008) 7043–7050, https://doi.org/10.1021/ac8011126.
[29] Z. Zhu, C. Huang, Q. He, Q. Xiao, Z. Liu, S. Zhang, S. Hu, On line vapor generation of osmium based on solution cathode glow discharge for the determination by ICP-OES, Talanta. 106 (2013) 133–136, https://doi.org/10.1016/j.talanta.2012.12.010.
[30] Z.A. Li, Q. Tan, X. Hou, K. Xu, C. Zheng, Single drop solution electrode glow discharge for plasma assisted-chemical vapor generation: sensitive detection of zinc and cadmium in limited amounts of samples, Anal. Chem. 86 (2014) 12093–12099, https://doi.org/10.1021/ac502911p.
[31] K. Greda, M. Gorska, M. Welna, P. Jamroz, P. Pohl, In-situ generation of ag, cd, hg, in, Pb, Tl and Zn volatile species by flowing liquid anode atmospheric pressure glow discharge operated in gaseous jet mode – evaluation of excitation processes and analytical performance, Talanta. 199 (2019) 107–115, https://doi.org/10.1016/j.talanta.2019.02.058.
[32] R.P. Yuri, Gas Discharge Physics - Y. P. Raizer.pdf, 1987.
[33] T. Cserfalvi, P. Mezei, Operating mechanism of the electrolyte cathode atmospheric glow discharge, Fresenius J. Anal. Chem. 355 (1996) 813–819, https://doi.org/10.1007/s0021663550813.
[34] C. De Izarra, UV OH spectrum used as a molecular pyrometer, J. Phys. D. Appl. Phys. 33 (2000) 1697–1704, https://doi.org/10.1088/0022-3727/33/14/309.
[35] P.J. Bruggeman, N. Sadeghi, D.C. Schram, V. Linss, Gas temperature determination from rotational lines in non-equilibrium plasmas: A review, Plasma Sources Sci. Technol. 23 (2014), https://doi.org/10.1088/0963-0252/23/2/023001.
[36] M.A. Gigosos, M.Á. González, V. Cardeñoso, Computer simulated Balmer-alpha, −beta and -gamma stark line profiles for non-equilibrium plasmas diagnostics, Spectrochim Acta Part B At Spectrosc. 58 (2003) 1489–1504, https://doi.org/10.1016/S0584-8547(03)00097-1.
[37] M.R. Webb, G.C.Y. Chan, F.J. Andrade, G. Gamez, G.M. Hieftje, Spectroscopic characterization of ion and electron populations in a solution-cathode glow discharge, J. Anal. At. Spectrom. 21 (2006) 525–530, https://doi.org/10.1039/b517418j.
[38] Y.J. Zhou, J. Ma, F. Li, T. Xian, Q.H. Yuan, Q.F. Lu, Sensitivity improvement of solution cathode glow discharge-optical emission spectrometry by external magnetic field for optical determination of elements, Microchem. J. 158 (2020), https://doi.org/10.1016/j.microc.2020.105224.
[39] K. Tachibana, K. Yasuoka, Understanding of chemical reactions induced by argon plasma in contact with sodium halide solutions: Importance of surface properties for plasma-liquid interactions, J. Phys. D. Appl. Phys. 53 (2020), https://doi.org/10.1088/1361-6463/ab5ebe.
[40] NIST Atomic Spectra Database, (n.d.). doi:10.18434/T4W30F.
[41] Y. Zhang, J. Orejas, J. Fandiño, D. Blanco Fernández, J. Pisonero, N. Bordel, Critical evaluation of SCGD-OES analytical performance in the presence of NaCl, J. Anal. At. Spectrom. (2022) 1150–1160, https://doi.org/10.1039/d1ja00439e.
[42] G. Jones, W.A. Ray, The surface tension of solutions of electrolytes as a function of the concentration. III, Sodium Chloride 63 (1909) 3262–3263.
[43] P. Kebarle, L. Tang, From ions in solution to ions in the gas phase, Anal. Chem. 65 (1993) 972A–986A, https://doi.org/10.1021/ac00070a715.